University of Reading

Anticancer evaluation of new organometallic ruthenium(II) flavone complexes

Article

Published Version

Creative Commons: Attribution 4.0 (CC-BY)

Open Access

Khater, M., Brazier, J. ORCID: https://orcid.org/0000-0002-4952-584X, Greco, F. and Osborn, H. ORCID: https://orcid.org/0000-0002-0683-0457 (2023) Anticancer evaluation of new organometallic ruthenium(II) flavone complexes. Medicinal Chemistry, 14 (2). pp. 253-267. ISSN 2632-8682 doi: 10.1039/D2MD00304J Available at https://centaur.reading.ac.uk/109188/

It is advisable to refer to the publisher's version if you intend to cite from the work. See Guidance on citing.

To link to this article DOI: http://dx.doi.org/10.1039/D2MD00304J

Publisher: Royal Society of Chemistry

All outputs in CentAUR are protected by Intellectual Property Rights law, including copyright law. Copyright and IPR is retained by the creators or other copyright holders. Terms and conditions for use of this material are defined in the End User Agreement.

www.reading.ac.uk/centaur

University of Reading

CentAUR

Central Archive at the University of Reading

Reading's research outputs online

RSC Medicinal Chemistry

ROYAL SOCIETY OF CHEMISTRY

RESEARCH ARTICLE

View Article Online
View Journal

Check for updates

Cite this: DOI: 10.1039/d2md00304j

Anticancer evaluation of new organometallic ruthenium(II) flavone complexes†

Mai Khater,[ab] John A. Brazier,[a] Francesca Greco*[a] and Helen M. I. Osborn *[a]

Received 2nd September 2022,
Accepted 22nd November 2022

DOI: 10.1039/d2md00304j

rsc.li/medchem

Targeting multiple malignancy features such as angiogenesis, proliferation and metastasis with one molecule is an effective strategy in developing potent anticancer agents. Ruthenium metal complexation to bioactive scaffolds is reported to enhance their biological activities. Herein, we evaluate the impact of Ru chelation on the pharmacological activities of two bioactive flavones (**1** and **2**) as anticancer candidates. The novel Ru complexes (**1Ru** and **2Ru**) caused a loss of their parent molecules' antiangiogenic activities in an endothelial cell tube formation assay. **1Ru** enhanced the antiproliferative and antimigratory activities of its 4-oxoflavone **1** on MCF-7 breast cancer cells (IC_{50} = 66.15 ± 5 μM and 50% migration inhibition, $p < 0.01$ at 1 μM). **2Ru** diminished 4-thioflavone's (**2**) cytotoxic activity on MCF-7 and MDA-MB-231 yet significantly enhanced **2**'s migration inhibition ($p < 0.05$) particularly on the MDA-MB-231 cell line. The test derivatives also showed non-intercalative interaction with VEGF and c-myc i-motif DNA sequences.

Open Access Article. Published on 15 December 2022. Downloaded on 1/20/2023 11:15:39 AM.
This article is licensed under a Creative Commons Attribution 3.0 Unported Licence.

1. Introduction

In spite of the current advances in cancer chemotherapy, treatment of metastatic tumours remains challenging. In that context, 90% of cancer related mortalities are caused by metastatic tumours rather than the primary malignant tissue.[1] Tumours rely on the constant formation of new blood vessels in order to grow and metastasize.[2] A proangiogenic switch plays a critical role in the growth of malignant tissues by increasing their supply of oxygen and nutrients. Additionally, increased angiogenesis promotes the invasive properties of dormant cancer cells which contributes to their metastatic profiles.[3] Since the discovery of the DNA binding agent cisplatin, the search for novel metal-based anticancer agents has evolved towards the development of less toxic versions of metal-based anticancer drugs with high efficacy and lower susceptibility to resistance.[4] Ruthenium based compounds in particular have gained special interest due to their desirable pharmacological properties such as high potency, low toxicity and low predisposition to resistance.[5,6] The Ru(III) organometallic compounds NAMI-A[7] and KP1019[8] were the first Ru metal-based derivatives to reach cancer clinical trials and display strong *in vivo* antimetastatic and anticancer activities, respectively[9] (Fig. 1). Despite the preliminary encouraging results, both NAMI-A and KP1019 did not proceed further with clinical trials due to toxicity and solubility issues.[5]

In depth research on the mechanisms of action of Ru(III) metal complexes showed that they are activated *in vivo via* reduction of the inert Ru(III) to the more toxic state, Ru(II).[10,11] Owing to their lower oxidation states, Ru(II) derivatives are more thermodynamically and kinetically stable than Ru(III) complexes.[12,13] Consequently, the attention of researchers has shifted towards the direct use of the active Ru(II) organometallic complexes especially in the form of arene-Ru(II) complexes. The unique half sandwich stool geometry and [η^6-arene-Ru(II)-XYZ] formula of arene-Ru complexes provides valuable structural features for medicinal chemistry programmes. For example, the arene ring, which comprises the seat part of the stool conformation, can increase cellular uptake of the metal complex by increasing its lipophilicity. X and Y are either one bidentate or two

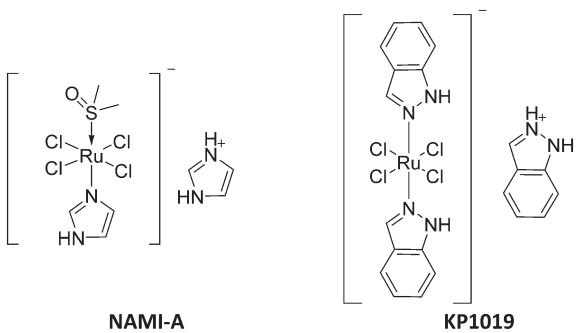

Fig. 1 Chemical structures of NAMI-A and KP1019.

[a] School of Pharmacy, University of Reading, Whiteknights, Reading, RG6 6AD, UK. E-mail: f.greco@reading.ac.uk, h.m.i.osborn@reading.ac.uk
[b] Therapeutic Chemistry Department, Pharmaceutical & Drug Industries Research Division, National Research Centre, Cairo, Egypt

† Electronic supplementary information (ESI) available. See DOI: https://doi.org/10.1039/d2md00304j

Open Access Article. Published on 15 December 2022. Downloaded on 1/20/2023 11:15:39 AM.
This article is licensed under a Creative Commons Attribution 3.0 Unported Licence.

monodentate ligands and together with Z (a leaving group, such as a halogen) they constitute the legs of the stool conformation.[14–16] Structural tuning of any part of the pharmacophore (*i.e.* the arene ring, the ligand and the leaving group) can alter the biological activity of the entire complex and its mode of action. *O*,*O*-Chelated-ruthenium complexes are widely reported for their cytotoxic and antimetastatic activities.[14,17,18] Pettinari *et al.* reported *in vitro* cytotoxic effects of biphenyl pyrazolonate based, and curcumin based, *O*,*O*-chelated ruthenium complexes in two studies.[19,20] The pyrazolonate derivatives showed activities comparable to that of cisplatin on cervical, breast, hepatocellular and colorectal cancer cell lines (IC_{50} values of 9–34 μM compared to 13–52 μM for cisplatin)[19] while the curcumin based complexes exhibited higher potency and cancer cell selectivity than cisplatin on ovarian cancer cell lines (IC_{50} values of 0.14–1.18 μM compared to 1.5–25 μM for cisplatin).[20]

Natural products have made many valuable contributions in the field of cancer drug discovery. For example, plant based drugs such as vincristine, paclitaxel and irinotecan have formed an integral part of cancer treatment regimens.[21] Flavonoids are polyphenolic chromone based compounds of natural origin and are capable of coordinating with metal atoms *via* their OH and/or C=O groups. Given the well reported anticancer and antiangiogenic properties of flavonoids,[22,23] their *O*,*O*-chelation with the bioactive Ru(II)-*p*-cymene moiety in a hybrid organometallic molecule may result in synergistic effects and enhance the pharmacological activities of both scaffolds.[24,25] In fact, Ru metal chelation to flavonoids has been shown to enhance some of their therapeutic effects in several studies.[24,26] Kurzwernhart *et al.*, for instance, reported better cytotoxic activity of a series of *p*-cymene-Ru(II)-flavonol complexes than their unsubstituted flavonols on a range of cancer cell lines.[27] However, in some cases no added benefits were observed in terms of activity after complexation hence a further study is warranted in this area to fully probe this phenomenon.

The study reported herein examined the effect of *p*-cymene-Ru(II) metal complexation on the *in vitro* antiangiogenic, antiproliferative, antimetastatic and DNA binding activities of the flavones (**1** and **2**). Compound **2** is a 4-thioflavone that showed significant *in vitro* antiproliferative, antiangiogenic and VEGFR2 phosphorylation inhibition activities in our previous studies.[23,28–30] Furthermore, the 4-oxoflavone (**1**) was included in the study to gain additional insight on the contribution of the functional group at position number 4 not only on the free flavonoid's activity but also on the biological effects of complexation. Initially, a tube formation assay was utilised for the synthetic derivatives (**1** and **2**) alongside the novel complexes (**1Ru** and **2Ru**) to establish their antiangiogenic potential on endothelial cells which are major contributors to the spread and growth of tumours. The direct effects of the synthesized compounds on malignant cells' proliferation were evaluated *via* cytotoxicity studies on the estrogen receptor positive (MCF-7) and the triple negative (MDA-MB-231) breast cancer cell lines. Due to the key role of cell migration in cancer metastasis, antimigratory activities of the flavone parents and the corresponding Ru(II) complexes were assessed on both the MCF-7 cell line and the invasive MDA-MB-231 cell line. Structure activity relationships (SAR) and dose response associations were also examined to gain insight on the antimigratory behaviour of these ruthenium metal derivatives and their parent flavones. Binding interactions of the synthetic flavone derivatives with the telomere i-motif forming sequences of VEGF and c-myc oncogenes (overexpressed in many cancers) were studied *via* UV-visible and DNA melting spectroscopy. I-motif DNA sequences are presumably capable of regulating oncogene expression and therefore are of interest for their anticancer applications.[31,32]

2. Results and discussion

2.1. Synthesis

The novel Ru (η^6-*p*-cymene) flavone complexes **1Ru** and **2Ru** were synthesized *via* the reaction of their parent flavones **1** and **2**, respectively, with the commercially available bis[Ru(η^6-*p*-cymene)Cl_2] following the deprotonation of **1** and **2** by sodium methoxide (NaOMe) in methanol (Scheme 1) based on the reported method.[16] The 4-C=O and 4-C=S ruthenium derivatives (**1Ru** and **2Ru**) were purified by crystallization in 9 : 1 ethyl acetate (EtOAc) : acetonitrile (ACN) or EtOAc : chloroform ($CHCl_3$), respectively, in 30% and 46% yields. Structures of the synthesized organometallic complexes **1Ru** and **2Ru** were confirmed by ^{1}H and ^{13}C NMR spectroscopic analysis, infrared spectroscopy, mass spectrometry, and elemental analysis. The ^{1}H NMR spectrum of **1Ru** showed the appearance of the *p*-cymene CH_3 protons peaks at δ 1.29, 1.30 and 2.17 ppm in addition to a multiplet corresponding to the CH proton at 2.84 ppm. Furthermore, aromatic protons of the cymene ring appeared as two doublets at δ 5.37 and 5.66 ppm (J = 7.2 Hz). Successful chelation of **1** and Ru(II)-*p*-cymene was also reinforced by the upfield shift of all of the proton signals of compound **1** with the ring A protons (H-6 and 8) seeing the highest shifts by 0.3 and 0.45 ppm, respectively. The peak of the 5-OH group proton where the chelation occurred was no longer present in **1Ru**'s ^{1}H NMR spectrum. Likewise, the ^{1}H NMR spectrum of **2Ru** exhibited the same patterns of successful complexation where signals of the *p*-cymene protons appeared at δ 1.16 and 1.18 (2xCH_3), 2.26 (CH_3), 2.83 (CH), 7.07 and 7.11 (Ar–CH) ppm in addition to the thioflavone moiety protons that were slightly shifted upfield and the disappearance of the 5-OH proton (ESI† Fig. S1B).

Fig. S3 and Table S1 in the ESI† document show the UV-vis stability profiles of the synthesized complexes **1Ru** and **2Ru** where they've shown minor spectral changes upon temperature increments indicating sufficient stability.

The carbon signals for the *p*-cymene ring were visible in both the aliphatic and aromatic regions along with the *p*-chlorophenyl ring carbons of the flavone moiety in the ^{13}C

 This journal is © The Royal Society of Chemistry 2022

Open Access Article. Published on 15 December 2022. Downloaded on 1/20/2023 11:15:39 AM.
This article is licensed under a Creative Commons Attribution 3.0 Unported Licence.

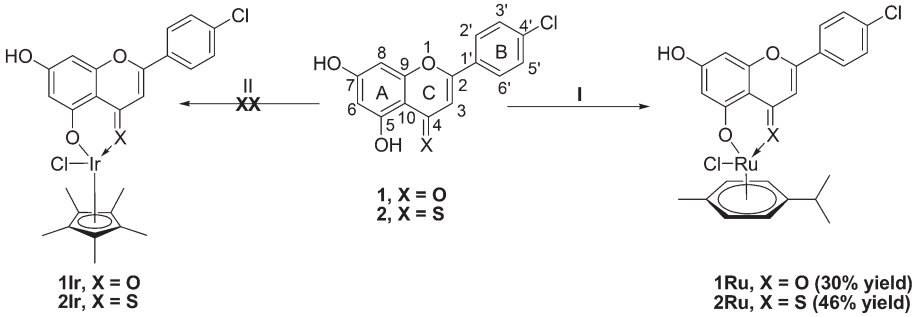

Scheme 1 Synthesis of Ru(II) flavone and thioflavone derivatives. (I) NaOMe, $[Ru(\eta^6\text{-}p\text{-cymene})Cl_2]_2$ in anhydrous DCM, MeOH, 75 °C, 18 h; (II) NaOMe, $[Ir(\eta^5\text{-Cp*})Cl_2]_2$ in anhydrous DCM, MeOH, 75 °C, 18 h.

NMR spectra of both complexes. For complex **1Ru** for instance, the ^{13}C NMR spectrum showed peaks corresponding to the CH_3 and CH groups of cymene at δ 17.92, 22.52 and 30.89 ppm in addition to the aromatic cymene carbons at δ 102.70, 106.34 and 129.81 ppm whereas a downfield shift of the flavone peaks was observed especially with ring A and C carbons (C8, 6, 3 and 5). The 4-C═O group signal also shifted from δ 181.83 to 177.55 ppm in the ^{13}C NMR spectrum of **1Ru**.

Attempts to synthesize the corresponding iridium(III) derivatives of flavones **1** and **2** did not afford the desired products. Following the same synthetic route detailed for the successful synthesis of the ruthenium(II) complexes, **1** and **2** were activated by deprotonation with NaOMe and this was followed by the addition of bis$[Ir(\eta^5\text{-Cp*})Cl_2]$ *in situ*. Interestingly, the ^1H NMR spectrum of **1Ir** showed 2 signals for the 5xCH_3 protons of the Cp* ring at δ 1.55 and 1.64 ppm and those corresponding to the flavone scaffold as well (ESI† Fig. S2A). This finding was previously reported for the related Ir(III)chrysin[33] and indicates the afforded product is a mixture of **1Ir** complex and starting material, or a mixture of the bidentate and monodentate Ir(III)-flavone complexes making its purification attempts unsuccessful. Although ^1H NMR spectroscopic analysis of the 4-thioflavone complex (**2Ir**) demonstrated successful chelation with a singlet signal for the 5xCH_3 protons of the Cp* ring at δ 1.64 ppm, in addition to the expected flavone moiety proton peaks (ESI† Fig. S2B), its CHN elemental analysis mainly corresponded to the bisdichlorido(η^5-Cp*)iridium(III) starting material indicating failed complexation.

2.2. Cytotoxicity on HUVEC cells

The biocompatibility of flavones (**1** and **2**)[30] alongside their ruthenium(II) metal complexes (**1Ru** and **2Ru**) with HUVEC cells was established using the trypan blue exclusion assay. A concentration four times higher (*i.e.* 40 μM) than the highest concentration used for the tube formation antiangiogenic evaluation study (*i.e.* 10 μM) was selected for this cytotoxic assay. Fig. 2 shows that the tested compounds retained ~100% viability of the cells with no statistically significant differences from the control ($p > 0.05$) indicating suitability of the test concentration (10 μM) for the antiangiogenic evaluation using HUVEC cells.

2.3. *In vitro* tube formation assay

In our recent study,[30] the 4′-chlorophenylflavone derivatives **1** and **2** have shown promising antiangiogenic activities *in vitro*. Herein, the effect of complexation with a ruthenium(II) metal ligand on the antiangiogenic activity of **1** and **2** was evaluated using the Matrigel tube formation assay that assesses many of the main steps involved in the process of angiogenesis. Inhibition of VEGF-mediated tube formation by the tested substrates was observed after 12 h of treatment on HUVECs at 1 μM and 10 μM concentrations. Luteolin is a natural flavone well known for its high antiangiogenic activity both *in vitro* and *in vivo*[34] and as such was used in this study as a reference standard. In accordance with reported data, luteolin inhibited the measured elements of tube formation by 30% compared to the positive control.[34,35] As seen in Fig. 3, the 4-thio-flavone-ruthenium complex **2Ru**, exhibited significant reduction in the number of junctions (40%, $p < 0.01$) and both the number and length of master segments (35%, $p < 0.05$) at 10 μM. As for the carbonyl complex (**1Ru**), even though it showed some antiangiogenic activity at 10 μM (overall tube formation inhibition = 22%), the observed effects were insignificant ($p > 0.05$) across all

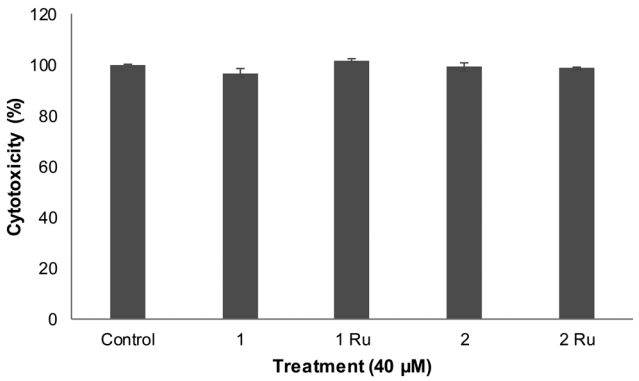

Fig. 2 Cell viability of HUVECs at 40 μM of tested flavones. Data are expressed as mean ± standard error of the mean (SEM), $n = 3$.

Open Access Article. Published on 15 December 2022. Downloaded on 1/20/2023 11:15:39 AM.
This article is licensed under a Creative Commons Attribution 3.0 Unported Licence.

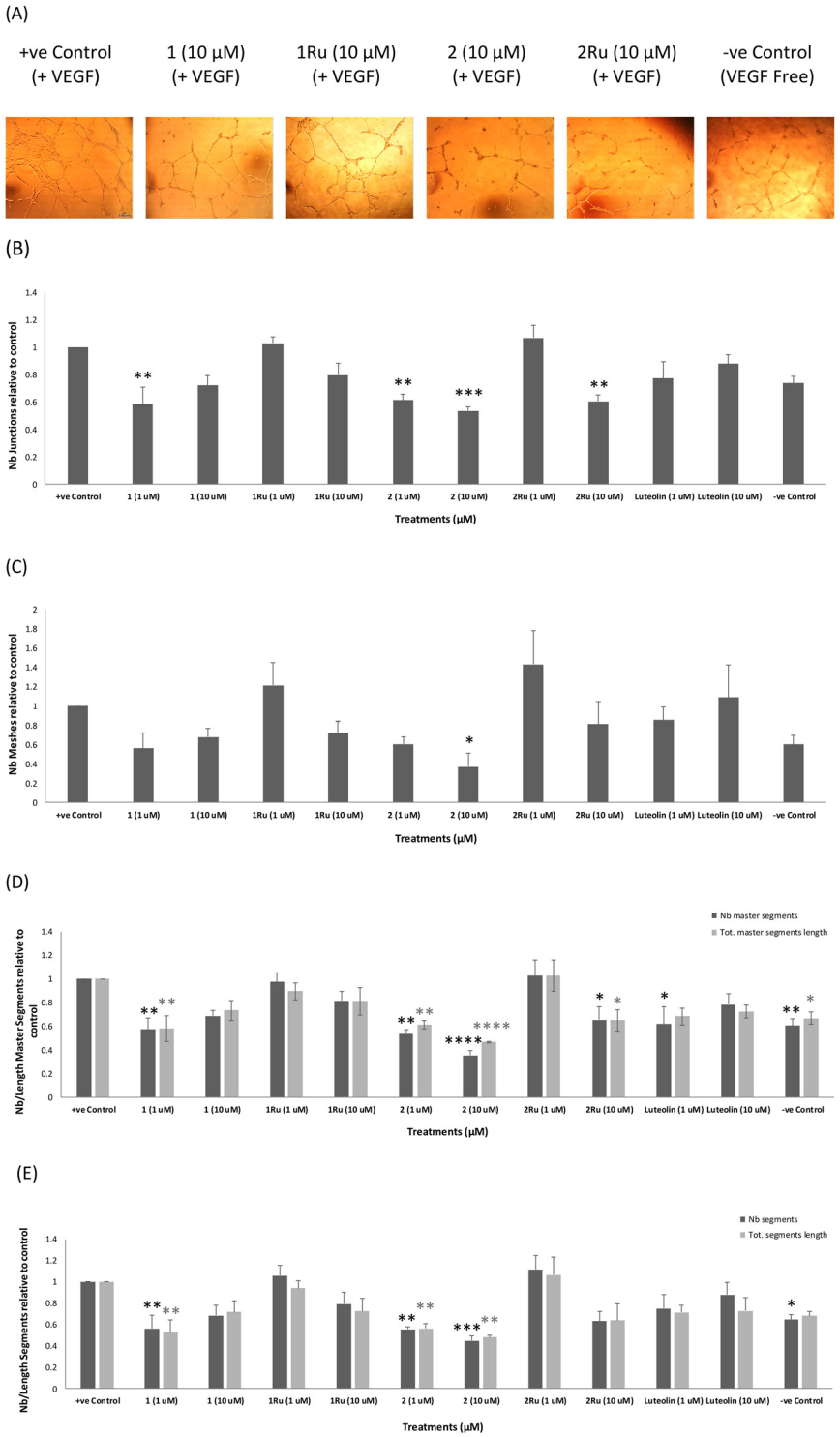

Fig. 3 Antiangiogenic activity of Ru(II) complexes (**1Ru** and **2Ru**) compared to the reported activity of their parent flavones (**1** and **2**) on *in vitro* HUVEC tube formation after 12 h expressed as a ratio to the +ve control (10 ng mL^{-1} VEGF-enriched media). (A) Representative images of tube formation assay at 4× magnification. Images were analysed using angiogenesis analyzer macro in ImageJ software; (B) number of junctions, (C) number of meshes; (D) number and length of master segments, (E) number and length of segments. Data are expressed as mean ± standard error of the mean (SEM), $n = 3$. Statistical significance was estimated with respect to the +ve control by one-way ANOVA, followed by Dunnett's multiple comparison test (*$p < 0.05$, **$p < 0.01$, ***$p < 0.001$, ****$p < 0.0001$).

the measured elements of tube formation. Meanwhile, both complexes **1Ru** and **2Ru** showed a total loss of their parents' tube formation inhibition activity at 1 µM (Fig. 3). In our latest study, compound **2** was shown to mediate its

 This journal is © The Royal Society of Chemistry 2022

Open Access Article. Published on 15 December 2022. Downloaded on 1/20/2023 11:15:39 AM. This article is licensed under a Creative Commons Attribution 3.0 Unported Licence.

antiangiogenic effects mainly *via* interaction with the VEGF/VEGFR2 pathway where the 4-C═S had a key role in the interaction with VEGFR2 and subsequent inhibition of its phosphorylation.[30] In this regard, complexation of a Ru(II) ligand at the 4-C═S group of compound **2** might have masked its desirable effect and lead to an altered binding mode with VEGFR2 which resulted in the significant reduction in activity seen upon complexation. The ability of Ru(II) organometallic derivatives to target tumour metastasis has been widely reported both *in vitro* and *in vivo*.[3,6,9,36] Thus, based on the preliminary antiangiogenic trends observed for our target Ru(II) complexes (**1Ru** and **2Ru**) and their parent flavones (**1** and **2**), we further investigated their antiproliferative and antimetastatic potential on the estrogen receptor positive breast cancer cell line (MCF-7) and the more aggressive triple negative cell line (MDA-MB-231).

2.4. Cell viability study

The unique chemical features and coordination geometries of metal ions can add several additional binding interactions that can potentially enhance their anticancer properties for example by allowing intercalation and exploitation of their redox potential.[24] Lead compound (**2**) has previously exhibited promising anticancer activity on several cancer cell lines in the low μM range.[29] In that context, coordination of derivative (**2**) with a Ru(II) metal ligand is a promising approach to further improve its antiproliferative activity. Likewise, structural modification of the inactive flavone (**1**) *via* ruthenium complexation can presumably result in a new lead with higher activity. Hence, the cytotoxic activities and IC_{50} values of complexes (**1Ru** and **2Ru**) and flavones (**1** and **2**) were measured by a 72 h MTT assay using a maximum concentration of 100 μM.

As shown in Fig. 4A, free flavone (**1**) showed no cytotoxic activity above 100 μM on the two breast cancer cell lines whereas its Ru(II) complex (**1Ru**) showed enhanced antiproliferative activity but only on the estrogen receptor positive cell line (MCF-7) with an IC_{50} of 66.15 ± 5 μM. In contrast, complex **2Ru** diminished the high antiproliferative activity observed for derivative **2** on the MCF-7 breast cancer cell line (IC_{50} = 1.2 ± 0.8 μM) and the moderate activity on the triple negative MDA-MB-231 cell line (IC_{50} = 43.06 ± 1.29 μM) (Fig. 4B, Table 1). Since substitution of the 4-C═O with 4-C═S group is the only structural difference between compound **1** and **2**, the S atom is likely to be critical for compound **2**'s cytotoxic activity. This observation explains, in part, the loss of the cytotoxic activity that occurred after complexation with Ru in complex **2Ru** as complexation might have hindered the S atom's ability to interact with its cellular target(s). The negative impact that masking of the 4-C═S group had was also demonstrated earlier when probing the antiangiogenic activity of **2Ru** *via* the tube formation assay. Moreover, several ruthenium organometallic complexes, such as NAMI-A, have similarly shown low potency in *in vitro* cytotoxicity studies while exhibiting remarkable antimetastatic effects *in vivo*.[14,37] Hence, the antimetastatic

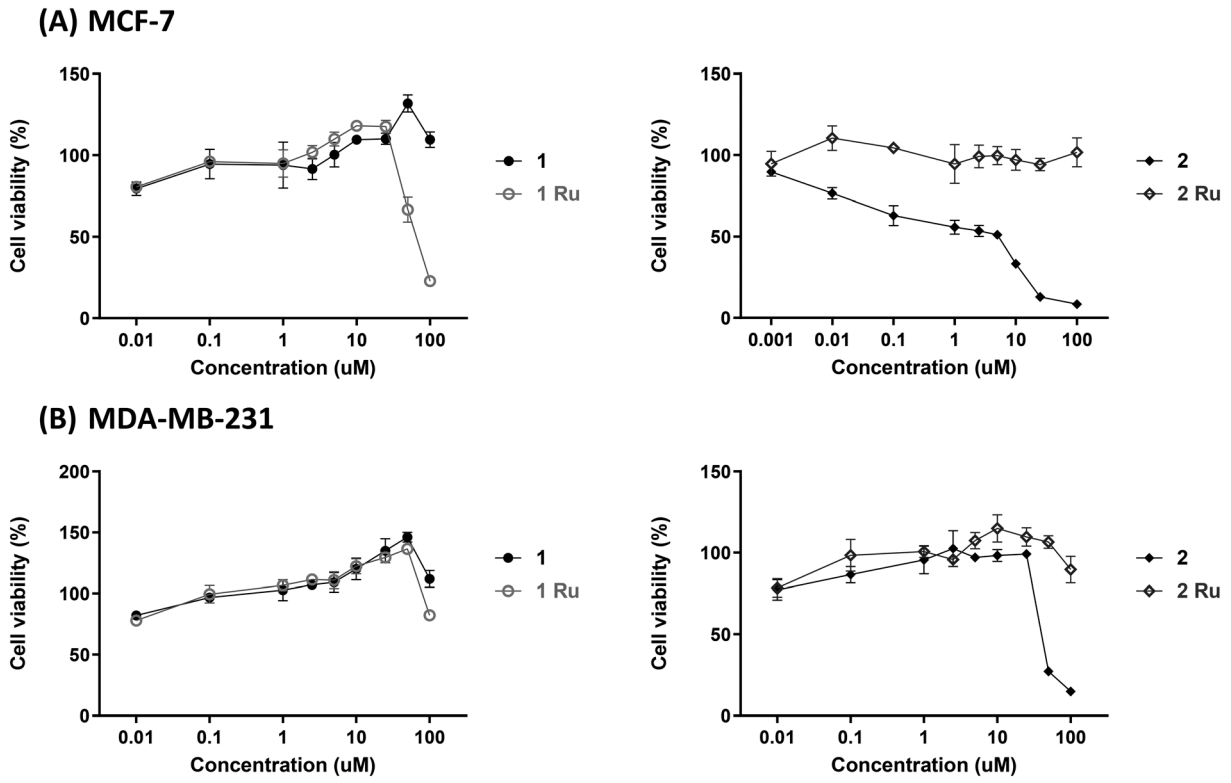

Fig. 4 Antiproliferative activity of flavone derivatives (**1** and **2**) and their Ru(II) complexes (**1Ru** and **2Ru**) against (A) MCF-7 and (B) MDA-MB-231 cancer cell lines. Data are expressed as mean ± standard error of the mean (SEM), n = 3.

Open Access Article. Published on 15 December 2022. Downloaded on 1/20/2023 11:15:39 AM.
This article is licensed under a Creative Commons Attribution 3.0 Unported Licence.

Table 1 Determined IC_{50} for flavone derivatives (**1** and **2**) and their Ru(II) complexes (**1Ru** and **2Ru**) against MCF-7 and MDA-MB-231. Data are expressed as mean ± standard error of the mean (SEM), $n = 3$

	IC_{50} (μM)	
Compound	MCF-7	MDA-MB-231
1	>100	>100
1Ru	66.15 ± 5	>100
2	1.2 ± 0.8	43.06 ± 1.29
2Ru	>100	>100

potential of complexes **1Ru** and **2Ru** in addition to their free flavones **1** and **2**, was evaluated by measuring their effects on breast cancer cells' migration.

2.5. Wound healing (migration) assay

Malignant cell migration is essential for tumour invasion and metastasis.[1] Thus, the ability of the synthetic flavones (**1** and **2**) and their Ru(II) metal complexes (**1Ru** and **2Ru**) to inhibit the migration of breast cancer cells (MCF-7 and MDA-MB-231) was assessed by an *in vitro* 24 h scratch assay. Low, sub-cytotoxic concentrations of 1, 10 and 20 μM were used in this evaluation. Given the high toxicity of compound **2** on the MCF-7 cell line (IC_{50} = 1.2 ± 0.8 μM), it was not possible to measure its antimigratory effects on that cell line. The 4-thioflavone ruthenium complex (**2Ru**), showed 55% migration inhibition of MCF-7 cells at 20 μM ($p < 0.001$) which is the highest activity observed on this cancer cell line (Fig. 5). **2Ru**'s high activity continued to be significant even at the lower concentrations of 1 and 10 μM (52% and 49% inhibition, respectively, $p < 0.01$). As seen in Fig. 5B, the improvement of the antimigratory activity of compound **1** upon complexation was prominent as there were no observed effects for the parent flavone at any of the tested doses. In that regard, complex **1Ru** exhibited significant reduction ($p < 0.01$) in MCF-7 cells' migration at all the tested concentrations with 50%, 42% and 41% inhibition at 1, 10 and 20 μM, respectively.

Results of the wound healing assay on the invasive breast cancer cell line (MDA-MB-231) showcased the antimigratory potency of complex **2Ru**. This is highlighted by a 47% fall in MDA-MB-231's migration ($p < 0.001$) relative to the control at low levels of 1 μM (Fig. 6). **2Ru** sustained its high activity at the higher 10 and 20 μM concentrations although to a lower extent (migration inhibition = 44%, $p < 0.01$ and 36%, $p < 0.05$, respectively). In terms of the biological effect of metal coordination, it resulted in a statistically significant rise in

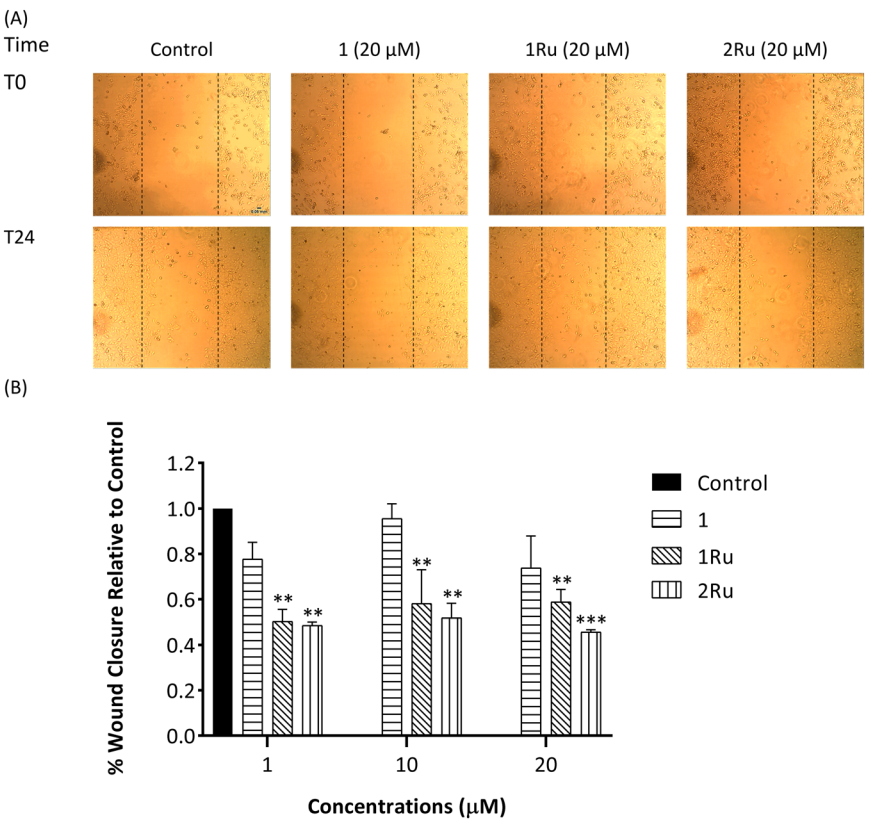

Fig. 5 *In vitro* MCF-7 wound closure (migration) inhibition activity of flavone derivative (**1**) and the Ru(II) complexes (**1Ru** and **2Ru**) expressed as a ratio to control. (A) Representative images of scratch assay at 0 h and 24 h at 4× magnification. Images were analysed using ImageJ software; (B) % wound closure after 24 h as a ratio to the control. Data are expressed as mean ± standard error of the mean (SEM), $n = 3$. Statistical significance was estimated with respect to the +ve control by one-way ANOVA, followed by Dunnett's multiple comparison test (**$p < 0.01$, ***$p < 0.001$).

This journal is © The Royal Society of Chemistry 2022

Open Access Article. Published on 15 December 2022. Downloaded on 1/20/2023 11:15:39 AM.
This article is licensed under a Creative Commons Attribution 3.0 Unported Licence.

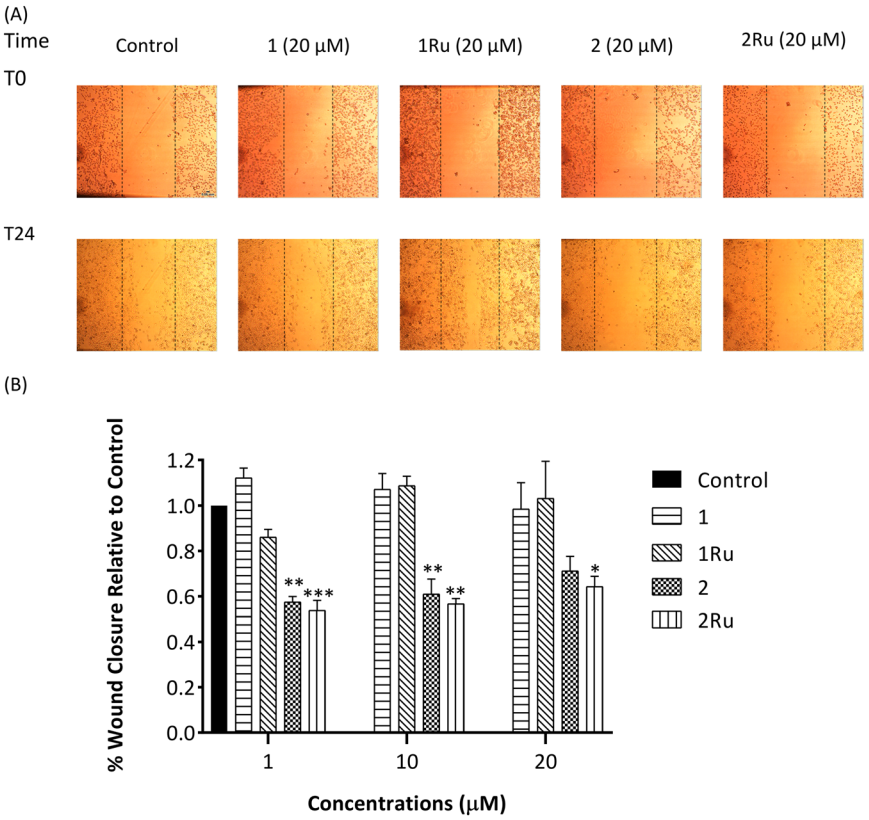

Fig. 6 *In vitro* MDA-MB-231 wound closure (migration) inhibition activity of flavone derivatives (**1** and **2**) and their Ru(II) complexes (**1Ru** and **2Ru**) expressed as a ratio to control. (A) Representative images of scratch assay at 0 h and 24 h at 4× magnification. Images were analysed using ImageJ software; (B) % wound closure after 24 h as a ratio to the control. Data are expressed as mean ± standard error of the mean (SEM), $n = 3$. Statistical significance was estimated with respect to the +ve control by one-way ANOVA, followed by Dunnett's multiple comparison test (*$p < 0.05$, **$p < 0.01$, ***$p < 0.001$).

compound **2**'s activity of 4% and 7% ($p < 0.05$) at 1 and 20 μM, respectively. For the 4-carbonyl derivative (**1**) and its Ru(II) complex (**1Ru**), neither showed any effect on the migration of MDA-MB-231 breast cancer cells indicating **1Ru**'s selectivity on MCF-7 cancer cell line. From a structure–activity relationship perspective, these findings suggest that the 4-thio group and the Ru(II) *p*-cymene ligands improve the antimigration activity of this panel of flavones and their structural features are therefore favourable over their 4-carbonyl or un-complexed flavones. Replacement of the 4-C═O with a 4-C═S functionality has been widely reported to enhance many of the pharmacological activities attributed to flavones such as neuroprotective, anticancer and antimicrobial activities.[29,38] The cymene-Ru(II) moiety also add several benefits to the chelated ligand as mentioned earlier. Thus combination of the S atom with the Ru(II)-arene presumably leads to better interaction with target proteins *via* several ways such as increasing the lipophilicity of the ligand.[30,39]

The observed trends in antimigratory activities on both breast cancer cell lines were not concentration dependant. As shown in Fig. 7, the effects the tested compounds had on cell migration were largely comparable across the range of the different concentrations used. Data from the wound healing assay on the MCF-7 cell line (Fig. 7A) suggested that activities were at their highest levels at 1 μM, slightly decreased at the 10 μM then increased at 20 μM. With the exception of flavone **1**, the highest activities on the inhibition of MDA-MB-231 cells' migration occurred at the lowest dose of 1 μM (Fig. 7B) where it was significantly higher ($p < 0.05$) in case of both **2** and **2Ru** compared to their activities at 20 μM. Previous studies have reported a negative dose–response relationship of flavonoids or their metabolites on their cell adhesion and antiangiogenic effects.[30,40] However, further investigations are still needed to unfathom the algorithms of this dosage-activity interplay.

2.6. I-motif DNA binding study

I-motifs are four stranded antiparallel cytosine rich DNA sequences capable of forming at telomere and promotor regions of genomic DNA.[41,42] I-motifs were initially thought to form in only acidic pH conditions, however they have recently been shown to form at physiological pH.[43] Due to the presence of potential i-motif forming sequences in 69% of promoter regions in human oncogenes, they are postulated to play a key role in oncogene expression regulation.[44] VEGF and c-myc i-motif sequences are prevalent in oncogene promotor regions

Open Access Article. Published on 15 December 2022. Downloaded on 1/20/2023 11:15:39 AM.
This article is licensed under a Creative Commons Attribution 3.0 Unported Licence.

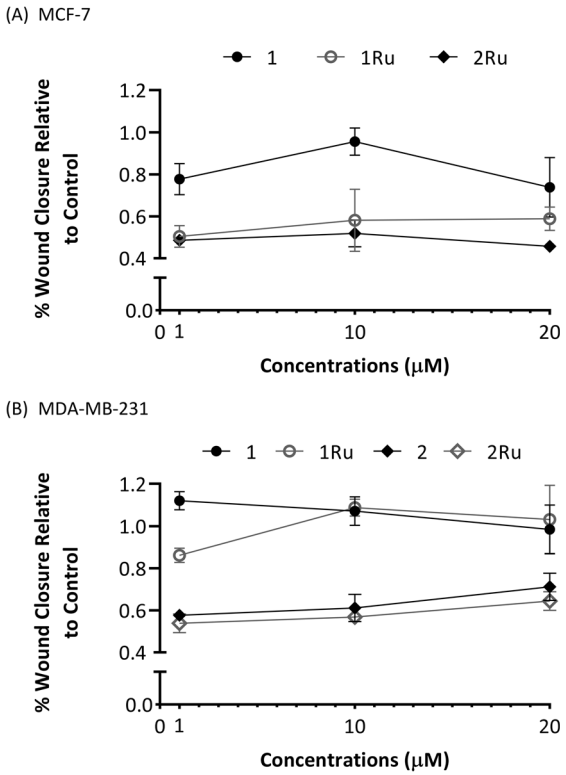

Fig. 7 Dose response trend lines of flavone derivative (**1**) and the Ru(II) complexes (**1Ru** and **2Ru**) at 1, 10 and 20 μM concentration. (A) MCF-7; (B) MDA-MB-231.

in many cancers including breast cancer and as such their ligands have potential anticancer roles.[45] The natural flavonol, fisetin, is reported to specifically bind to VEGF i-motif DNA and regulate its function by stabilizing its hairpin structure.[31] Similarly, Ru-based complexes exhibited i-motif binding properties.[46,47] In continuation of our investigation of the effects of Ru metal complexation on the different biological activities of flavonoids, interactions with VEGF and c-myc i-motif DNA were studied using UV-vis spectroscopic techniques. Fig. 8 shows the absorption spectra of VEGF and c-myc i-motif sequences with or without flavones (**1** and **2**) and their Ru complexes (**1Ru** and **2Ru**) in DNA : flavonoid equimolar ratios (2 μM : 2 μM). The thioflavone (**2**) exhibited the most pronounced effects on the absorbance maximum (λ_{max}) of VEGF and c-myc i-motifs with 16% and 18% hyperchromic shifts, respectively. Ruthenium metal complexation to compound **2** had a negative influence on its i-motif DNA interaction where **2Ru** showed 2% and 8% increase in λ_{max} of VEGF and c-myc sequences, respectively. However, **2Ru**'s addition led to a 1 nm hypsochromic shift of VEGF i-motif absorbance maximum from 272 to 271 nm. On the other hand, addition of the 4-oxo flavone (**1**) and its Ru complex (**1Ru**) led to minor changes in λ_{max} of both sequences that was hypochromic (5% and 3%) with VEGF and hyperchromic (2% and 5%) in case of c-myc (Fig. 8).

The effect of this set of flavones on VEGF and c-myc was further evaluated *via* thermal stability measurements. Stabilizing/destabilizing the promotor i-motif structures is often reported to regulate expression of the corresponding genes, which for VEGF and c-myc could have detrimental effects on cancer growth and propagation.[48] As observed in Fig. 9, effects of the test flavones on the thermal stability of the VEGF and c-myc i-motif sequences were generally marginal and in agreement with λ_{max} chromophoric shifts. Complex **2Ru**, resulted in the highest effect seen on VEGF i-motif by destabilizing the sequence as indicated by 4 °C decrease in the i-motif's transition temperature (T_m) (Table 2). A similar destabilization was observed for the same complex (**2Ru**) on c-myc however much less pronounced. Compound **1** destabilized VEGF i-motif in contrast to stabilizing the c-myc one. This mirrored the

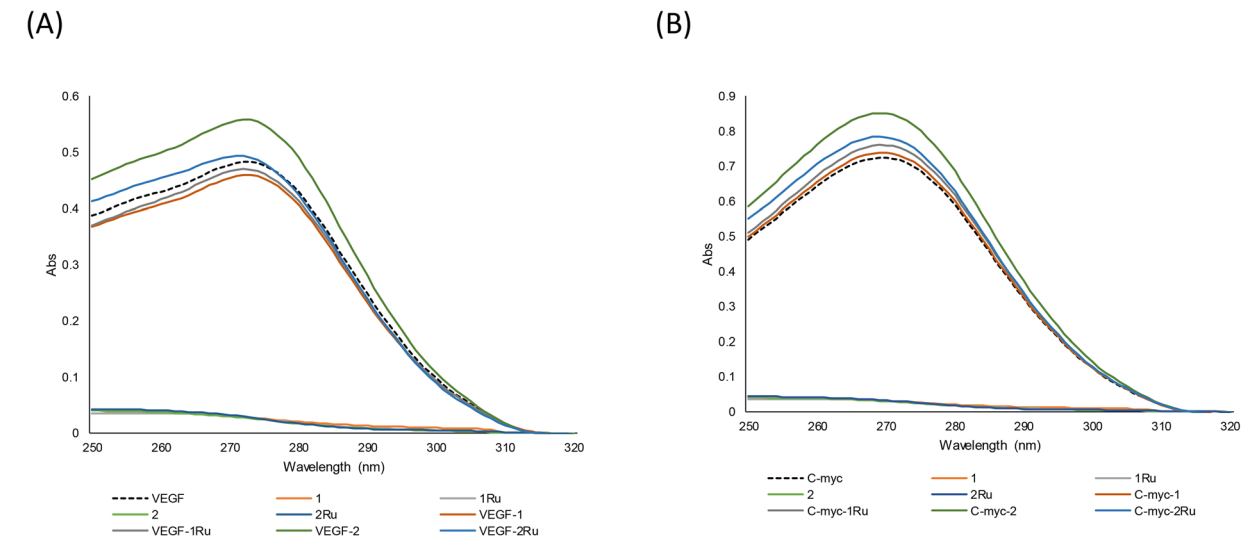

Fig. 8 Absorption spectra of VEGF and c-myc I motif DNA with flavones (**1**, **1Ru**, **2** and **2Ru**) in 1 : 1 ratio. (A) VEGF i-motif interactions; (B) C-myc i-motif interactions.

This journal is © The Royal Society of Chemistry 2022

Open Access Article. Published on 15 December 2022. Downloaded on 1/20/2023 11:15:39 AM.
This article is licensed under a Creative Commons Attribution 3.0 Unported Licence.

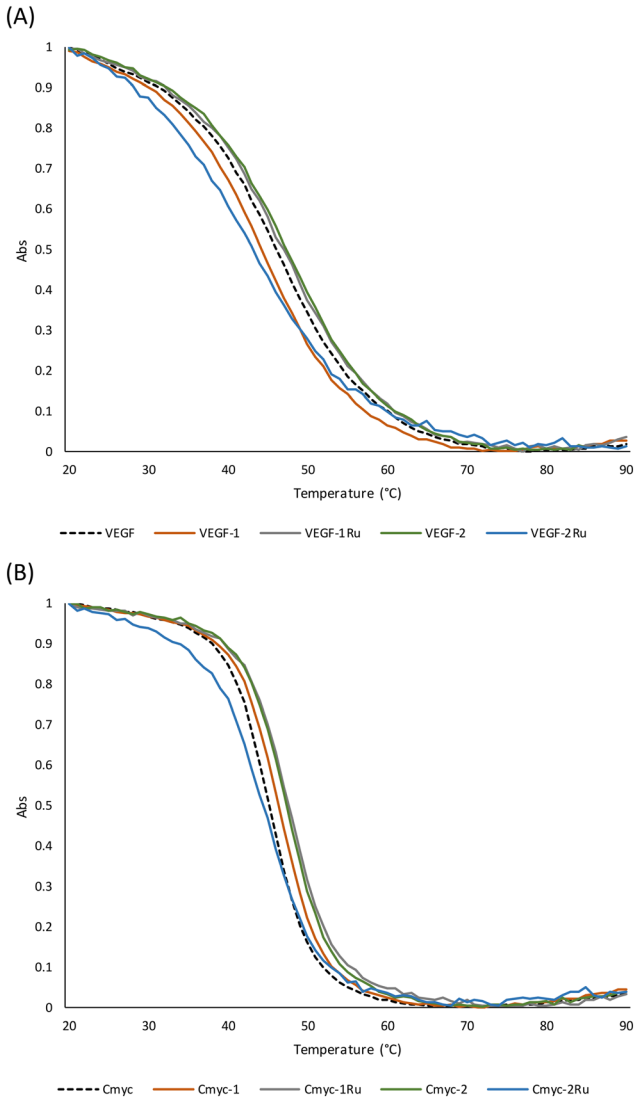

Fig. 9 Normalized UV melting curves for VEGF and c-myc i-motif DNA with flavones (**1**, **1Ru**, **2** and **2Ru**) at 295 nm at 1 : 1 ratio. (A) VEGF i-motif melt; (B) C-myc i-motif melt.

trend of a higher chromophoric shift observed for flavone **1** with VEGF i-motif sequence that also differed in pattern (hypochromic) from the shift witnessed with the c-myc sequence (hyperchromic). These findings could indicate higher selectivity of the 4-oxo derivative (**1**) towards VEGF i-motif based on an intercalative binding mode especially that hypochromic shifts are reported with DNA intercalation.[49,50] In contrast to its parent, complex **1Ru** showed a smaller stabilization effect (1 °C) on VEGF compared to c-myc i-motif (3 °C) again echoing the λ_{max} shifts. In this regard, the highest i-motif activity seen for the parent flavonoids was switched from VEGF to c-myc with compound **1** and *vice versa* with compound **2** upon Ru chelation. This emphasizes the key role of the interplay between the substitution at position 4 and metal complexation on the interaction with biological targets.

Previous studies have reported small changes of the T_m value of i-motif sequences with terbium (Tb) and Ru complexes in spite of good binding affinity to the target i-motif DNA. Two amino acid-Tb complexes were shown to bind to i-motif at 22 and 30 μM while having ΔT_m of −0.5 and −4 °C, respectively.[51] A polypyridyl-Ru complex also showed high affinity to i-motif DNA at 5.6 μM while showing no effect on the thermal stability of the i-motif.[47] Hence, despite the minor effects observed for the test flavones and their Ru complexes on i-motifs' absorbance and thermal stability, they might be indicative of some level of DNA interaction. A small increase or decrease, similar to that observed with this panel of flavone derivatives, in absorbance at λ_{max} is often attributed to a non-intercalative or external binding mode to DNA that is weaker in comparison to intercalation.[52,53] Such external DNA binding has previously been reported for Ru complexes since the presence of a metal atom facilitates external DNA binding by electrostatic interaction with the negatively charged phosphate groups of DNA base pairs.[24,46,47,52] Moreover, only a limited number of i-motif ligands have been identified throughout the literature which is often attributed to the difficulty of stacking of planar molecules inside the i-motif's compact structure.[32] This further supports the hypothesis that the tested panel of flavone derivatives mainly display non-intercalative binding modes.

3. Conclusion

The influence of Ru metal complexation on the biological activities of parent flavonoids is somewhat controversial. While some reports show enhanced activities, others indicate no significant benefits upon complexation. In this study, two novel Ru(II)-flavone complexes (**1Ru** and **2Ru**) were synthesized and different aspects of their anticancer

Table 2 T_m[a] and ΔT_m[b] of VEGF and c-myc i-motifs in the presence of flavones (**1**, **1Ru**, **2** and **2Ru**) at 1 : 1 ratio

VEGF i-motif	T_m (°C)	ΔT_m (°C)	C-myc i-motif	T_m (°C)	ΔT_m (°C)
VEGF	46	0	Cmyc	45	0
VEGF-**1**	44	−2	Cmyc-1	46	1
VEGF-**1Ru**	47	1	Cmyc-1Ru	48	3
VEGF-**2**	47	1	Cmyc-2	47	2
VEGF-**2Ru**	42	−4	Cmyc-2Ru	44	−1

[a] T_m is the midpoint of the transition from each melting experiment. [b] $\Delta T_m = T_{m\ (DNA\text{-}flavone)} - T_{m\ (DNA)}$.

Open Access Article. Published on 15 December 2022. Downloaded on 1/20/2023 11:15:39 AM. This article is licensed under a Creative Commons Attribution 3.0 Unported Licence.

effects (antiangiogenic, antiproliferative, antimetastatic and i-motif binding) were assessed in comparison to their parent flavones (**1** and **2**). In general, complexation had a detrimental effect on the endothelial cell antiangiogenic activities of the free flavones. Further investigations of the impact of Ru metal coordination on the cytotoxic and antimigratory activities of the flavones of focus on breast cancer cell lines (MCF-7 and MDA-MB-231) displayed interesting trends. The impact of Ru coordination on the antimetastatic capacity of compound **1** mirrored the effects seen on the antiproliferative activity, with **1Ru** displaying significantly enhanced activities for flavone **1** ($p < 0.01$), and improved selectively on the MCF-7 cell line. On the other hand, **2Ru** reduced the antiproliferative activity of its unchelated flavone (**2**) yet showed high inhibition of both breast cancer cells' migration which was significantly better than its parent **2** on the MDA-MB-231 cell line ($p < 0.05$). Interactions of flavones (**1** and **2**) and their Ru complexes (**1Ru** and **2Ru**) were also studied with VEGF and c-myc i-motif DNA using UV-vis spectroscopic techniques. The tested derivatives and their metal complexes have shown minor shifts in the absorption maxima and the transition temperatures of the i-motif sequences mostly indicating a non-intercalative mode of binding. These initial findings on the UV-vis effects of these flavones on VEGF and c-myc i-motif DNA sequences need further exploration in scope of the mode of interaction as well as the concentration and pH dependency of these effects. The patterns of activity resulting from the different assays used in this study highlight the important role of the 4-functional group on the antiangiogenic, cytotoxic, antimetastatic and DNA binding activities of the tested panel of derivatives. First of all, a positive role of the 4-C═S group was observed on the overall activity of this set of flavones with an additional benefit of Ru(II) complexation on the antimigratory activity. Secondly, the similarity between the cytotoxic and migration inhibition trends for **1Ru** suggest a common antiproliferative/antimetastatic target that is selective for MCF-7 cells. This is indeed opposed by the variability in these trends witnessed with the thiocarbonyl counterparts (**2** and **2Ru**) hence, proposing different antiproliferative/antimetastatic mechanisms of action that might be shared between both breast cancer cell lines. All in all, these results emphasized the constructive contribution of metal complexation on flavones' antimetastatic activities, and the fundamental role of the ligand's chelating atom as well as the nature of the studied pharmacological effect on the biological outcome. Hence, this study paves the way for the development of novel bi-modal anticancer/antimetastatic agents[54] that are able to combat both tumour growth and propagation. Such leads with dual activity are much needed in the fight against cancer since they allow for the use of fewer chemotherapeutic agents and consequently reduce the undesirable side effects and clinical implications of using combinations of different drugs. Moreover, they have better chances to overcome the acquired drug resistance which is a common limitation of many of the current chemotherapeutic agents.

4. Materials and methods

4.1. Chemicals, reagents and analytical methods

Chemicals, reagents and analytical grade solvents were purchased from Sigma-Aldrich (Gillingham, UK) unless specified. All reactions were carried out under argon. ^{1}H and ^{13}C NMR spectra were recorded in deuterated dimethyl sulfoxide (DMSO-d_6) using a Bruker DPX 400 (400 MHz) spectrometer where chemical shifts (δ) were reported as parts per million (ppm) relative to tetramethylsilane (TMS) as internal standard. Coupling constants (J) are reported in Hertz (Hz) and multiplicities are reported as follows: s (singlet), d (doublet), t (triplet), or m (multiplet). Infrared spectra were recorded on a Perkin Elmer precisely spectrum 100 FT-IR spectrometer. Mass spectrometry data were recorded on a Thermo Fisher LTQ Orbitrap XL instrument. CHN elemental analyses for metal compounds were obtained from MEDAC LTD (Woking, UK), analytical and consultancy services.

4.2. Cell culture

HUVECs were purchased from Sigma-Aldrich (ECACC) (Gillingham, UK) and cultured in EGM-2 medium (EBM with SingleQuotes™ kit: foetal bovine serum (FBS), fibroblast growth factor B, epidermal growth factor, vascular endothelial growth factor (VEGF), insulin-like growth factor-1, heparin, hydrocortisone) (Lonza, Belgium). MCF-7 (ER +ve breast cancer cell line, wild type) were purchased from Sigma-Aldrich (ECACC) (Gillingham, UK) and cultured in RPMI 1640 medium supplemented with 5% FBS (Fischer Scientific, Loughborough, UK). MDA-MB-231 (triple −ve breast cancer cell line) were purchased from Sigma-Aldrich (ECACC) (Gillingham, UK) and cultured in DMEM medium (1 g L^{-1} glucose, without L-glutamine) supplemented with 2% L-glutamine (200 mM) and 10% FBS (Fischer Scientific, Loughborough, UK). The cells were incubated at 37 °C and 5% CO_2. HUVEC cells were at passage 3–5 when used in the experiment and were not further sub-cultured. Bovine serum albumin (BSA) was purchased from Sigma Aldrich (Gillingham, UK). Recombinant human VEGFR-A165 was purchased from Peprotech (London, UK). Corning™ Matrigel™ GFR Membrane Matrix was purchased from (Fischer Scientific, Loughborough, UK). Reagents for phosphate buffered saline (PBS) for cell culture were purchased from Sigma Aldrich (Gillingham, UK). PBS (pH 7.4) was freshly prepared in lab and solution pH was checked before used. Images were captured using 1.3 M microscope digital eyepiece camera. ImageJ software was used to quantify tube formation and cell migration. The stock solutions of the test compounds (20 mM) were prepared in 100% sterile DMSO. These stocks were then appropriately diluted with the complete culture medium and DMSO levels were maintained below 0.1% in the test concentrations.

This journal is © The Royal Society of Chemistry 2022

Open Access Article. Published on 15 December 2022. Downloaded on 1/20/2023 11:15:39 AM. This article is licensed under a Creative Commons Attribution 3.0 Unported Licence.

4.3. I-motif DNA binding study

UV-visible absorbance measurements and DNA UV melting studies were performed on a Cary 300 C (Varian USA) UV-visible spectrophotometer. VEGF and c-myc i-motif DNA (5′-3′ sequences (CCCCGCCCCCGGCCCGCCCC) and (CCTTCCCCA CCCTCCCCACCCTCCCCA), respectively) were purchased from Sigma-Aldrich (Gillingham, UK) and used without further purification. Na cacodylate buffer (20 mM, pH 5.5) was used for both i-motifs. DNA concentrations were determined by measuring the absorbance at 260 nm after melting using the molar extinction coefficient supplied by the manufacturer. VEGF and c-myc i-motifs were prepared for experiments by diluting with buffer solution, annealed with or without the flavonoid at 95 °C for 5 min then gently cooled to room temperature. The stock solutions of the test compounds (20 mM) were prepared in 100% sterile DMSO. These stocks were then appropriately diluted with HPLC grade water and DMSO levels were maintained below 0.1% in the test concentrations.

4.4. Statistical analysis

Statistical analysis was carried out against the control group by one-way ANOVA followed by Dunnett's *post hoc* test using Graphpad Prism 6. Statistical significance value was set at $p < 0.05$.

4.5. Synthesis

Synthesis of the parent flavonoids (**1**) and (**2**) followed the previously published protocol.[30,33]

4.5.1. Synthesis of chlorido [(5-oxo-κO)-7-hydroxy-2-(4′-chlorophenyl)-4*H*-chromen-4-onato-κO] (η^6-*p*-cymene) ruthenium(II) (1Ru). A solution of NaOMe (28 mg, 0.525 mmol, 1.05 eq.) in 10 mL anhydrous MeOH was added to 2-(4-chlorophenyl)-5,7-dihydroxy-4*H*-chromen-4-one (**1**) (144 mg, 0.5 mmol) and the suspension was stirred at 50 °C for 30 min. $[Ru(\eta^6\text{-}p\text{-cymene})Cl_2]_2$ (168 mg, 0.275 mmol, 0.55 eq.) in 10 mL anhydrous DCM was added to the reaction mixture and this was stirred at 75 °C overnight under an argon atmosphere. The solvent was evaporated *in vacuo* and the residue was dissolved in 15 mL warm $CHCl_3$: MeOH (9 : 1) and filtered to remove any salts and impurities formed during the reaction. The filtrate was concentrated *in vacuo* to 2–3 mL and the product was precipitated by the addition of few drops of EtOAc. The formed precipitate was filtered, air dried and recrystallized from EtOAc : ACN (9 : 1) to give a bright red powder.

Yield: 30%; mp: decompose 230 °C; elemental analysis: found: C, 53.45; H, 4.12; Ru, 17.72. $C_{25}H_{22}Cl_2O_4Ru$ requires C, 53.77; H, 3.97; Ru, 18.10; IR ν_{max}/cm^{-1}: 3231 (OH, w, b), 1633 (C═O, v, s), 1094 (C–O, v, s); ^{1}H NMR: (400 MHz, DMSO-d_6, Me_4Si) δ 1.29 (3H, d, J = 2.4 Hz, CH_3 cym), 1.30 (3H, d, J = 2 Hz, CH_3 cym), 2.17 (3H, s, CH_3 cym), 2.81–2.88 (1H, m, CH cym), 5.37 (2H, d, J = 7.2 Hz, H-2, 6cym), 5.66 (2H, d, J = 7.2 Hz, H-3, 5cym), 5.99 (1H, d, J = 2.4 Hz, H-6), 6.05 (1H, d, J = 2 Hz, H-8), 7.00 (1H, s, H-3), 7.61 (2H, d, J = 8.4 Hz, H-2′, 6′), 8.05 (2H, d, J = 8.4 Hz, H-3′, 5′), 10.27 (1H, s, OH); ^{13}C NMR: (100 MHz, DMSO-d_6, Me_4Si) δ 17.92 (CH_3 cym), 22.52 (2xCH_3 cym), 30.89 (CH cym), 78.54 (C8), 82.86 (C6), 90.33 (C10), 97.08 (C3), 102.70 (C3, 5 cym), 106.34 (C2, 6 cym), 128.49 (C3′, 5′), 129.68 (C2′, 6′), 129.81 (C1, 4 cym), 158.58 (C2, 5), 168.09 (C7), 177.55 (C═O); m/z (FTMS + ESI): observed as M-Cl ($C_{25}H_{22}O_4{}^{35}ClRu$) requires 523.0250, found 523.0233.

4.5.2. Synthesis of chlorido [(5-oxo-κO)-7-hydroxy-2-(4′-chlorophenyl)-4*H*-chromen-4-thionato-κO] (η^6-*p*-cymene) ruthenium(II) (2Ru). A solution of NaOMe (28 mg, 0.525 mmol, 1.05 eq.) in 10 mL anhydrous MeOH was added to 2-(4-chlorophenyl)-5,7-dihydroxy-4*H*-chromene-4-thione (**2**) (152.37 mg, 0.5 mmol) and the suspension was stirred at 50 °C for 30 min. $[Ru(\eta^6\text{-}p\text{-cymene})Cl_2]_2$ (303 mg, 0.495 mmol, 0.9 eq.) in 10 mL anhydrous dichloromethane was added to the reaction mixture and stirred at 75 °C overnight under argon atmosphere. The solvent was evaporated *in vacuo* and the residue was dissolved in 15 mL warm $CHCl_3$: MeOH (9 : 1) and filtered to remove any salts and impurities formed during the reaction. The filtrate was concentrated *in vacuo* to 2–3 mL and the product was precipitated by the addition of few drops of EtOAc. The formed precipitate was filtered, air dried and recrystallized from EtOAc : $CHCl_3$ (9 : 1) to give a dark reddish brown powder.

Yield: 46%; mp: >360 °C; elemental analysis: found: C, 51.58; H, 3.85; Ru, 17.30. $C_{25}H_{22}Cl_2O_3RuS$ requires C, 52.27; H, 3.86; Ru, 17.59 (% of C content is >0.4% due to the presence of traces of chloroform); IR ν_{max}/cm^{-1}: 3141 (OH, w, b), 1173 (C═S, v, m), 1088 (C–O, v, m); ^{1}H NMR: (400 MHz, DMSO-d_6, Me_4Si) δ 1.16 (3H, s, CH_3 cym), 1.18 (3H, s, CH_3 cym), 2.26 (3H, s, CH_3 cym), 2.81–2.87 (1H, m, CH cym), 6.18 (1H, d, J = 2.4 Hz, H-6), 6.2 (1H, d, J = 2.4 Hz, H-8), 7.07 (2H, d, J = 8.4 Hz, H-2, 6 cym), 7.11 (2H, d, J = 8.4 Hz, H-3, 5 cym), 7.62 (1H, s, H-3), 7.64 (2H, d, J = 8.8 Hz, H-2′, 6′), 8.11 (2H, d, J = 8.8 Hz, H-3′, 5′), 10.57 (1H, s, OH); ^{13}C NMR: (100 MHz, DMSO-d_6, Me_4Si) δ 21.04 (CH_3 cym), 24.46 (2xCH_3 cym), 33.45 (CH cym), 93.00 (C8), 111.99 (C3), 126.56 (C1′, 3′, 5′), 128.49 (C4 cym), 129.28 (C2′, 6′), 129.81 (C1 cym), 135.03 (C4′), 145.78 (C2); m/z (FTMS + ESI): observed as M-Cl ($C_{25}H_{22}O_3S^{35}ClRu$) requires 539.0022, found 539.0062.

4.6. Biological assays

4.6.1. Cytotoxicity on HUVECs. Cytotoxic activity of treatments on HUVECs using trypan blue exclusion assay.[55] HUVECs were seeded in 96 well plates at 1×10^5 cells per mL and cultured for 24 h. Cells were then treated with either luteolin, the synthesised derivatives at 40 μM or culture medium (control) for 24 h. After 24 h, solutions were removed and cells washed with 100 μL PBS followed by the addition of 50 μL trypsin–EDTA and incubation for 5 min to detach the cells. 50 μL of EGM-2 media was added to the wells. 50 μL aliquots of the cell suspension were mixed with equal volume of trypan blue (TB) 0.2% v/v (prepared from 0.4% TB diluted with PBS) then the cells were counted using a haemocytometer. Number of viable and dead cells were counted manually and %

Open Access Article. Published on 15 December 2022. Downloaded on 1/20/2023 11:15:39 AM. This article is licensed under a Creative Commons Attribution 3.0 Unported Licence.

cell viability of each treatment was expressed as % of control using the equation:

$$\%\ \text{Cell Viability} = (\text{Cell viability in treatment}/\text{Cell viability in control}) \times 100$$

where cell viability was calculated as follows:

$$\text{Cell Viability} = \text{Number of viable cells}/\text{Total number of cells(viable and dead)}.$$

4.6.2. Endothelial cell tube formation assay. HUVECs were cultured until confluency and then serum starved (0.1% serum) for 24 h. The tube formation assay followed the reported assay.[56] Briefly, 96 well plates were coated with 50 μL of Corning™ Matrigel™ GFR Membrane Matrix at 4 °C and incubated at 37 °C for 1–2 h to solidify. Serum starved HUVECs were seeded on the solidified Matrigel at 3×10^5 cells per mL and treated with medium containing VEGF (10 ng mL^{-1}) and either luteolin or one of the synthesised derivatives (at 1 μM or 10 μM). Plates were incubated for 12 h and photos covering the whole well area were taken using 4× magnification power of an inverted light microscope. Number of junctions, number and length of segments and master segments were quantified from the taken Images *via* the Angiogenesis Analyzer plugin[57] in ImageJ software.[58] The Angiogenesis Analyzer plugin proved to be an efficient tool in characterizing the branching of endothelial cells into tube networks as well as identifying various elements of endothelial tube formation.[57] Data was represented as a ratio to the positive control (VEGF enriched).

4.6.3. Cell viability. MCF-7 and MDA-MB-231 cells were seeded at a density of 4×10^4 and 2×10^4 cells per mL, respectively, into 96 well plates and incubated to allow the attachment for 24 h. After 24 h, the cells were treated with one of the synthesised derivatives at range of concentrations (0–100 μM) for 67 h. After 67 h, 20 μL of MTT (5 mg mL^{-1}) solution in PBS was added to each well and the cells were incubated for 5 h. The purple crystals formed were dissolved in 100 μL of DMSO and the plates were read at 560 nm using a SPECTRA max UV spectrometer (Bio-Rad). The data represented are the mean of the three individual experiments.

4.6.4. Scratch assay. MCF-7 or MDA-MB-231 cells were seeded in 12-well plates at 2×10^5 or 1×10^5 cells per mL, respectively, and cultured until 70–80% confluency. Afterwards, they were serum-starved (0% serum) for 24 h to inactivate the cell proliferation. A scratch was performed on the cell monolayers using a 200 μL pipette tip. Cells were then washed twice with PBS and treated with complete medium and one of the synthesized derivatives at 1, 10 or 20 μM. Compound **2** was not tested on MCF-7 cell line due to cytotoxicity (IC_{50} = 1.2 μM). Images of the scratches were taken immediately after performing the scratch (t = 0 h) and at 24 h (t = 24 h). The area not covered by the cells was quantified using ImageJ software. % of wound closure was calculated using the following equation:

$$100 \times ((\text{Area of scratch at } t0 - \text{Area of scratch at } t24)/\text{Area of scratch at } t0)$$

4.6.5. I-motif DNA binding study. UV-visible absorbance measurements and UV melting studies of either free i-motifs (VEGF or c-myc), free flavone (**1**, **1Ru**, **2** or **2Ru**) or both i-motif DNA and flavone (2 μM: 2 μM) were recorded using 1.0 cm matched quartz cuvettes. First spectra were recorded in the range of 200–500 nm to determine the relevant wavelength range were no peaks were observed above 320 nm. Subsequent spectra were hence recorded in the range of 200–320 nm. UV-visible absorbance was measured at 25 °C while melting curves were collected at a heating rate of 1 °C min^{-1} from 20 to 90 °C. T_m was calculated by non-linear fitting of the sigmoidal curve obtained at 295 nm.

Conflicts of interest

There are no conflicts to declare.

Acknowledgements

We are grateful to the Newton-Mosharafa Fund, British council, Egypt for a scholarship that has funded M. K.'s PhD studies, and to the University of Reading for provision of the Chemical Analysis Facility. We are also thankful for the PhD student, Madonna Mitry, for carrying out some parts of the DNA binding study.

References

1 F. Entschladen, T. L. Drell VI, K. Lang, J. Joseph and K. S. Zaenker, Tumour-Cell Migration, Invasion, and Metastasis: Navigation by Neurotransmitters, *Lancet Oncol.*, 2004, **5**(4), 254–258, DOI: **10.1016/S1470-2045(04)01431-7**.

2 P. Carmeliet and R. K. Jain, Angiogenesis in Cancer and Other Diseases, *Nature*, 2000, **407**(6801), 249–257, DOI: **10.1038/35025220**.

3 H. Lai, Z. Zhao, L. Li, W. Zheng and T. Chen, Antiangiogenic Ruthenium (Ii) Benzimidazole Complexes, Structure-Based Activation of Distinct Signaling Pathways, *Metallomics*, 2015, **7**(3), 439–447, DOI: **10.1039/C4MT00312H**.

4 N. Muhammad and Z. Guo, Metal-Based Anticancer Chemotherapeutic Agents, *Curr. Opin. Chem. Biol.*, 2014, **19**(1), 144–153, DOI: **10.1016/J.CBPA.2014.02.003**.

5 K. Lin, Z. Z. Zhao, H. B. Bo, X. J. Hao and J. Q. Wang, Applications of Ruthenium Complex in Tumor Diagnosis and Therapy, *Front. Pharmacol.*, 2018, **9**, 1323–1332, DOI: **10.3389/FPHAR.2018.01323**.

6 L. Yang, J. Zhang, C. Wang, X. Qin, Q. Yu, Y. Zhou and J. Liu, Interaction between 8-Hydroxyquinoline Ruthenium(II) Complexes and Basic Fibroblast Growth Factors (BFGF): Inhibiting Angiogenesis and Tumor Growth through ERK and AKT Signaling Pathways, *Metallomics*, 2014, **6**(3), 518–531, DOI: **10.1039/c3mt00237c**.

7 J. M. Rademaker-Lakhai, D. Van Den Bongard, D. Pluim, J. H. Beijnen and J. H. M. Schellens, A Phase I and Pharmacological Study with Imidazolium-Trans-DMSO-

 This journal is © The Royal Society of Chemistry 2022

Open Access Article. Published on 15 December 2022. Downloaded on 1/20/2023 11:15:39 AM. This article is licensed under a Creative Commons Attribution 3.0 Unported Licence.

Imidazole-Tetrachlororuthenate, a Novel Ruthenium Anticancer Agent, *Clin. Cancer Res.*, 2004, **10**(11), 3717–3727, DOI: **10.1158/1078-0432.CCR-03-0746**.

8 C. G. Hartinger, M. A. Jakupec, S. Zorbas-Seifried, M. Groessl, A. Egger, W. Berger, H. Zorbas, P. J. Dyson and B. K. Keppler, KP1019, A New Redox-Active Anticancer Agent – Preclinical Development and Results of a Clinical Phase I Study in Tumor Patients, *Chem. Biodiversity*, 2008, **5**(10), 2140–2155, DOI: **10.1002/CBDV.200890195**.

9 C. M. Clavel, E. Păunescu, P. Nowak-Sliwinska, A. W. Griffioen, R. Scopelliti and P. J. Dyson, Discovery of a Highly Tumor-Selective Organometallic Ruthenium(II)-Arene Complex, *J. Med. Chem.*, 2014, **57**(8), 3546–3558, DOI: **10.1021/jm5002748**.

10 C. G. Hartinger, M. Groessl, S. M. Meier, A. Casini and P. J. Dyson, Application of Mass Spectrometric Techniques to Delineate the Modes-of-Action of Anticancer Metallodrugs, *Chem. Soc. Rev.*, 2013, **42**(14), 6186–6199, DOI: **10.1039/C3CS35532B**.

11 A. I. Minchinton and I. F. Tannock, Drug Penetration in Solid Tumours, *Nat. Rev. Cancer*, 2006, **6**(8), 583–592, DOI: **10.1038/nrc1893**.

12 L. Duan, A. Fischer, Y. Xu and L. Sun, Isolated Seven-Coordinate Ru(IV) Dimer Complex with [HOHOH]- Bridging Ligand as an Intermediate for Catalytic Water Oxidation, *J. Am. Chem. Soc.*, 2009, **131**(30), 10397–10399, DOI: **10.1021/JA9034686**.

13 M. Abid, F. Shamsi and A. Azam, Ruthenium Complexes: An Emerging Ground to the Development of Metallopharmaceuticals for Cancer Therapy, *Mini-Rev. Med. Chem.*, 2016, **16**(10), 772–786.

14 L. Zeng, P. Gupta, Y. Chen, E. Wang, L. Ji, H. Chao and Z. S. Chen, The Development of Anticancer Ruthenium(Ii) Complexes: From Single Molecule Compounds to Nanomaterials, *Chem. Soc. Rev.*, 2017, **46**(19), 5771–5804, DOI: **10.1039/C7CS00195A**.

15 S. Y. Lee, C. Y. Kim and T. G. Nam, Ruthenium Complexes as Anticancer Agents: A Brief History and Perspectives, *Drug Des., Dev. Ther.*, 2020, **14**, 5375–5392, DOI: **10.2147/DDDT.S275007**.

16 D. Ravishankar, M. Salamah, A. Attina, R. Pothi, T. M. Vallance, M. Javed, H. F. Williams, E. M. S. Alzahrani, E. Kabova, R. Vaiyapuri, K. Shankland, J. Gibbins, K. Strohfeldt, F. Greco, H. M. I. Osborn and S. Vaiyapuri, Ruthenium-Conjugated Chrysin Analogues Modulate Platelet Activity, Thrombus Formation and Haemostasis with Enhanced Efficacy, *Sci. Rep.*, 2017, **7**(1), 1–16, DOI: **10.1038/s41598-017-05936-3**.

17 A. Habtemariam, M. Melchart, R. Fernández, S. Parsons, I. D. H. Oswald, A. Parkin, F. P. A. Fabbiani, J. E. Davidson, A. Dawson, R. E. Aird, D. I. Jodrell and P. J. Sadler, Structure-Activity Relationships for Cytotoxic Ruthenium(II) Arene Complexes Containing N,N-, N,O-, and O, O-Chelating Ligands, *J. Med. Chem.*, 2006, **49**(23), 6858–6868, DOI: **10.1021/JM060596M**.

18 C. M. Clavel, E. Păunescu, P. Nowak-Sliwinska, A. W. Griffioen, R. Scopelliti and P. J. Dyson, Modulating the Anticancer Activity of Ruthenium(II)-Arene Complexes, *J. Med. Chem.*, 2015, **58**(8), 3356–3365, DOI: **10.1021/JM501655T**.

19 R. Pettinari, C. Pettinari, F. Marchetti, B. W. Skelton, A. H. White, L. Bonfili, M. Cuccioloni, M. Mozzicafreddo, V. Cecarini, M. Angeletti, M. Nabissi and A. M. Eleuteri, Arene-Ruthenium(II) Acylpyrazolonato Complexes: Apoptosis-Promoting Effects on Human Cancer Cells, *J. Med. Chem.*, 2014, **57**(11), 4532–4542, DOI: **10.1021/JM500458C**.

20 R. Pettinari, F. Marchetti, F. Condello, C. Pettinari, G. Lupidi, R. Scopelliti, S. Mukhopadhyay, T. Riedel and P. J. Dyson, Ruthenium(II)-Arene RAPTA Type Complexes Containing Curcumin and Bisdemethoxycurcumin Display Potent and Selective Anticancer Activity, *Organometallics*, 2014, **33**(14), 3709–3715, DOI: **10.1021/OM500317B**.

21 A. G. Desai, G. N. Qazi, R. K. Ganju, M. El-Tamer, J. Singh, A. K. Saxena, Y. S. Bedi, S. C. Taneja and H. K. Bhat, Medicinal Plants and Cancer Chemoprevention, *Curr. Drug Metab.*, 2008, **9**(7), 581–591, DOI: **10.2174/138920008785821657**.

22 D. Ravishankar, A. K. Rajora, F. Greco and H. M. I. Osborn, Flavonoids as Prospective Compounds for Anti-Cancer Therapy, *Int. J. Biochem. Cell Biol.*, 2013, **45**(12), 2821–2831, DOI: **10.1016/j.biocel.2013.10.004Review**.

23 M. Khater, F. Greco and H. M. I. Osborn, Antiangiogenic Activity of Flavonoids: A Systematic Review and Meta-Analysis, *Molecules*, 2020, **25**(20), 4712–4742, DOI: **10.3390/molecules25204712**.

24 M. Khater, D. Ravishankar, F. Greco and H. M. I. Osborn, Metal Complexes of Flavonoids: Their Synthesis, Characterization and Enhanced Antioxidant and Anticancer Activities, *Future Med. Chem.*, 2019, **11**(21), 2845–2867, DOI: **10.4155/fmc-2019-0237**.

25 A. C. Munteanu, A. Notaro, M. Jakubaszek, J. Cowell, M. Tharaud, B. Goud, V. Uivarosi and G. Gasser, Synthesis, Characterization, Cytotoxic Activity, and Metabolic Studies of Ruthenium(II) Polypyridyl Complexes Containing Flavonoid Ligands, *Inorg. Chem.*, 2020, **59**(7), 4424–4434, DOI: **10.1021/ACS.INORGCHEM.9B03562**.

26 M. Małecka, A. Skoczyńska, D. M. Goodman, C. G. Hartinger and E. Budzisz, Biological Properties of Ruthenium(II)/(III) Complexes with Flavonoids as Ligands, *Coord. Chem. Rev.*, 2021, **436**, 213849–213869, DOI: **10.1016/J.CCR.2021.213849**.

27 A. Kurzwernhart, W. Kandioller, S. Bächler, C. Bartel, S. Martic, M. Buczkowska, G. Mühlgassner, M. A. Jakupec, H. B. Kraatz, P. J. Bednarski, V. B. Arion, D. Marko, B. K. Keppler and C. G. Hartinger, Structure-Activity Relationships of Targeted RuII(η 6- P -Cymene) Anticancer Complexes with Flavonol-Derived Ligands, *J. Med. Chem.*, 2012, **55**(23), 10512–10522, DOI: **10.1021/jm301376a**.

28 D. Ravishankar, K. A. Watson, S. Y. Boateng, R. J. Green, F. Greco and H. M. I. I. Osborn, Exploring Quercetin and Luteolin Derivatives as Antiangiogenic Agents, *Eur. J. Med. Chem.*, 2015, **97**, 259–274, DOI: **10.1016/j.ejmech.2015.04.056**.

Open Access Article. Published on 15 December 2022. Downloaded on 1/20/2023 11:15:39 AM. This article is licensed under a Creative Commons Attribution 3.0 Unported Licence.

29 D. Ravishankar, K. A. Watson, F. Greco and H. M. I. Osborn, Novel Synthesised Flavone Derivatives Provide Significant Insight into the Structural Features Required for Enhanced Anti-Proliferative Activity, *RSC Adv.*, 2016, **6**(69), 64544–64556, DOI: **10.1039/c6ra11041j**.

30 M. Khater, K. A. Watson, S. Y. Boateng, F. Greco and H. M. I. Osborn, Halogenated Flavonoid Derivatives Display Antiangiogenic Activity, *Molecules*, 2022, **27**(15), 4757–4778.

31 S. Takahashi, S. Bhattacharjee, S. Ghosh, N. Sugimoto and S. Bhowmik, Preferential Targeting Cancer-Related i-Motif DNAs by the Plant Flavonol Fisetin for Theranostics Applications, *Sci. Rep.*, 2020, **10**(1), 1–13, DOI: **10.1038/s41598-020-59343-2**.

32 S. Benabou, A. Aviñó, R. Eritja, C. González and R. Gargallo, Fundamental Aspects of the Nucleic Acid I-Motif Structures, *RSC Adv.*, 2014, **4**(51), 26956–26980, DOI: **10.1039/C4RA02129K**.

33 D. Ravishankar, Design, Synthesis and Biological Evaluation of Novel Flavone Derivatives, *PhD*, University of Reading, 2015.

34 P. Pratheeshkumar, Y. O. Son, A. Budhraja, X. Wang, S. Ding, L. Wang, A. Hitron, J. C. Lee, D. Kim, S. P. Divya, G. Chen, Z. Zhang, J. Luo and X. Shi, Luteolin Inhibits Human Prostate Tumor Growth by Suppressing Vascular Endothelial Growth Factor Receptor 2-Mediated Angiogenesis, *PLoS One*, 2012, **7**(12), 52279, DOI: **10.1371/journal.pone.0052279**.

35 X. Li, M. Chen, X. Lei, M. Huang, W. Ye, R. Zhang and D. Zhang, Luteolin Inhibits Angiogenesis by Blocking Gas6/Axl Signaling Pathway, *Int. J. Oncol.*, 2017, **51**(2), 677–685, DOI: **10.3892/ijo.2017.4041**.

36 P. Nowak-Sliwinska, J. R. Van Beijnum, A. Casini, A. A. Nazarov, G. Wagnières, H. Van Den Bergh, P. J. Dyson and A. W. Griffioen, Organometallic Ruthenium(II) Arene Compounds with Antiangiogenic Activity, *J. Med. Chem.*, 2011, **54**(11), 3895–3902, DOI: **10.1021/JM2002074**.

37 S. Zorzet, A. Bergamo, M. Cocchietto, A. Sorc, B. Gava, E. Alessio, E. Iengo and G. Sava, Lack of In Vitro Cytotoxicity, Associated to Increased G 2-M Cell Fraction and Inhibition of Matrigel Invasion, May Predict In Vivo-Selective Antimetastasis Activity of Ruthenium Complexes, *J. Pharmacol. Exp. Ther.*, 2000, **295**(3), 927–933.

38 J. Dong, Q. Zhang, Q. Meng, Z. Wang, S. Li and J. Cui, The Chemistry and Biological Effects of Thioflavones, *Mini-Rev. Med. Chem.*, 2018, **18**(20), 1714–1732, DOI: **10.2174/1389557518666180515145633**.

39 P. A. Ragazzon, J. Iley and S. Missailidis, Structure-Activity Studies of the Binding of the Flavonoid Scaffold to DNA, *Anticancer Res.*, 2009, **29**(6), 2285–2293.

40 K. Beekmann, L. Actis-Goretta, P. J. Van Bladeren, F. Dionisi, F. Destaillats and I. M. C. M. Rietjens, A State-of-the-Art Overview of the Effect of Metabolic Conjugation on the Biological Activity of Flavonoids, *Food Funct.*, 2012, **3**(10), 1008–1018, DOI: **10.1039/C2FO30065F**.

41 H. A. Day, P. Pavlou and Z. A. E. Waller, I-Motif DNA: Structure, Stability and Targeting with Ligands, *Bioorg. Med. Chem.*, 2014, **22**(16), 4407–4418, DOI: **10.1016/j.bmc.2014.05.047**.

42 H. A. Assi, M. Garavís, C. González and M. J. Damha, I-Motif DNA: Structural Features and Significance to Cell Biology, *Nucleic Acids Res.*, 2018, **46**(16), 8038–8056, DOI: **10.1093/nar/gky735**.

43 J. Brazier, A. Shah and G. B.-C. Communications, 2012, U. I-Motif Formation in Gene Promoters: Unusually Stable Formation in Sequences Complementary to Known G-Quadruplexes, *Chem. Commun.*, 2012, **48**(87), 10739–10741.

44 J. L. Huppert and S. Balasubramanian, G-Quadruplexes in Promoters throughout the Human Genome, *Nucleic Acids Res.*, 2007, **35**(2), 406–413, DOI: **10.1093/NAR/GKL1057**.

45 S. L. Brown and S. Kendrick, The I-Motif as a Molecular Target: More Than a Complementary DNA Secondary Structure, *Pharmaceuticals*, 2021, **14**(2), 96–120, DOI: **10.3390/PH14020096**.

46 S. Shi, X. Geng, J. Zhao, T. Yao, C. Wang, D. Yang, L. Zheng and L. Ji, Interaction of [Ru(Bpy)2(Dppz)]2+ with Human Telomeric DNA: Preferential Binding to G-Quadruplexes over i-Motif, *Biochimie*, 2010, **92**(4), 370–377, DOI: **10.1016/J.BIOCHI.2010.01.003**.

47 S. Shi, J. Zhao, X. Geng, T. Yao, H. Huang, T. Liu, L. Zheng, Z. Li, D. Yang and L. Ji, Molecular "Light Switch" for G-Quadruplexes and i-Motif of Human Telomeric DNA: [Ru(Phen)2(Dppz)]2+, *Dalton Trans.*, 2010, **39**(10), 2490–2493, DOI: **10.1039/B916094A**.

48 S. S. Masoud and K. Nagasawa, I-Motif-Binding Ligands and Their Effects on the Structure and Biological Functions of I-Motif, *Chem. Pharm. Bull.*, 2018, **66**(12), 1091–1103, DOI: **10.1248/cpb.c18-00720**.

49 P. Ross and S. Subramanian, Thermodynamics of Protein Association Reactions: Forces Contributing to Stability, *Biochemistry*, 1981, **20**(11), 3096–3102.

50 N. Sohrabi, Binding And UV/Vis Spectral Investigation of Interaction of Ni(II) Piroxicam Complex With Calf Thymus Deoxyribonucleic Acid (Ct-DNA) : A Thermodynamic Approach, *J. Pharm. Sci. Res.*, 2015, **7**(8), 533–537.

51 H. Xu, H. Zhang and X. Qu, Interactions of the Human Telomeric DNA with Terbium–Amino Acid Complexes, *J. Inorg. Biochem.*, 2006, **100**(10), 1646–1652, DOI: **10.1016/J.JINORGBIO.2006.05.015**.

52 T. Biver, Use of UV-Vis Spectrometry to Gain Information on the Mode of Binding of Small Molecules to DNAs and RNAs, *Appl. Spectrosc. Rev.*, 2012, **47**(4), 272–325, DOI: **10.1080/05704928.2011.641044**.

53 L. Hassani, Z. Fazeli, E. Safaei, H. Rastegar and M. Akbari, A Spectroscopic Investigation of the Interaction between C-MYC DNA and Tetrapyridinoporphyrazinatozinc(II), *J. Biol. Phys.*, 2014, **40**(3), 275–283, DOI: **10.1007/S10867-014-9348-X**.

54 R. Kerbel and J. Folkman, Clinical Translation of Angiogenesis Inhibitors, *Nat. Rev. Cancer*, 2002, **2**(10), 727–739, DOI: **10.1038/nrc905**.

55 A. L. Acton, C. Fante, B. Flatley, S. Burattini, I. W. Hamley, Z. Wang, F. Greco and W. Hayes, Janus PEG-Based Dendrimers for Use in Combination Therapy: Controlled Multi-Drug Loading and Sequential Release, *Biomacromolecules*, 2013, **14**(2), 564–574, DOI: **10.1021/bm301881h**.

56 Endothelial Cell Tube Formation Assay | Thermo Fisher Scientific – UK, **https://www.thermofisher.com/uk/en/home/**

 This journal is © The Royal Society of Chemistry 2022

references/protocols/cell-and-tissue-analysis/cell-profilteration-assay-protocols/angiogenesis-protocols/endothelial-cell-tube-formation-assay.html#prot4 (accessed Oct 18, 2021).
57 Angiogenesis Analyzer for ImageJ - Gilles Carpentier Research Web Site: Computer Image Analysis, https://image.bio.methods.free.fr/ImageJ/?Angiogenesis-Analyzer-for-ImageJ (accessed Oct 18, 2021).
58 W. S. Rasband, ImageJ. U.S. National Institutes of Health: Bethesda, Maryland, U.S.A.

Open Access Article. Published on 15 December 2022. Downloaded on 1/20/2023 11:15:39 AM.
This article is licensed under a Creative Commons Attribution 3.0 Unported Licence.